OPEN

# 7 T Musculoskeletal MRI
## Fundamentals and Clinical Implementation

*Shila Pazahr, MD,\*† Daniel Nanz, PhD,†‡ and Reto Sutter, MD\*†*

**Abstract:** This review summarizes the current state-of-the-art of musculoskeletal 7 T magnetic resonance imaging (MRI), the associated technological challenges, and gives an overview of current and future clinical applications of [1]H-based 7 T MRI. The higher signal-to-noise ratio at 7 T is predominantly used for increased spatial resolution and thus the visualization of anatomical details or subtle lesions rather than to accelerate the sequences. For musculoskeletal MRI, turbo spin echo pulse sequences are particularly useful, but with altered relaxation times, B1 inhomogeneity, and increased artifacts at 7 T; specific absorption rate limitation issues quickly arise for turbo spin echo pulse sequences. The development of dedicated pulse sequence techniques in the last 2 decades and the increasing availability of specialized coils now facilitate several clinical musculoskeletal applications. 7 T MRI is performed in vivo in a wide range of applications for the knee joint and other anatomical areas, such as ultra-high-resolution nerve imaging or bone trabecular microarchitecture imaging. So far, however, it has not been shown systematically whether the higher field strength compared with the established 3 T MRI systems translates into clinical advantages, such as an early-stage identification of tissue damage allowing for preventive therapy or an influence on treatment decisions and patient outcome. At the moment, results tend to suggest that 7 T MRI will be reserved for answering specific, targeted musculoskeletal questions rather than for a broad application, as is the case for 3 T MRI. Future data regarding the implementation of clinical use cases are expected to clarify if 7 T musculoskeletal MRI applications with higher diagnostic accuracy result in patient benefits compared with MRI at lower field strengths.

**Key Words:** MRI, 7 T, musculoskeletal, artifacts, MR physics, knee, nerves, foot, fingers

(*Invest Radiol* 2023;58: 88–98)

The spatial resolution of clinical magnetic resonance imaging (MRI) of the musculoskeletal system has substantially increased over the last 3 decades, driven by the advent of 3 T magnets with higher signal-to-noise ratios (SNRs) and the widespread availability of dedicated high-end extremity coils.[1] For many clinical questions in musculoskeletal medicine, MRI at 1.5 T and 3 T field strength can provide adequate answers, which has led to significant improvements in patient care.[2] Now, with the advent of clinical 7 T scanners, new possibilities for musculoskeletal imaging arise.

## ULTRA-HIGH-FIELD MUSCULOSKELETAL MRI

The first ultra-high-field magnets, that is, the MRI scanners with a main magnetic field strength (B0) of 7 T and above, were introduced

more than 2 decades ago, with 1 system operating at 7 T and another at 8 T field strength,[3,4] although research magnets with field strengths above 3 T had been installed many years earlier. However, the clinical implementation of ultra-high-field scanners is a slow process that has only recently gained speed. Several artifacts, particularly related to chemical shift and signal intensity inhomogeneities, only have a limited impact at 1.5 T and 3 T but can substantially deteriorate image quality at 7 T and higher field strengths.[5,6]

Although at lower field strengths, 2-dimensional (2D) turbo spin echo (TSE) sequences are the mainstay of musculoskeletal MRI due to their good in-plane resolution, excellent tissue-border depiction, and contrast-to-noise ratio (CNR), the quality of TSE images acquired at 7 T was, for many years, inferior to those from 3 T MRI.[7,8] Several gradient echo imaging studies demonstrated the feasibility of 7 T to image the bone microarchitecture to the level of individual trabeculae but were impaired by marked signal inhomogeneities throughout the field of view, especially in the soft tissues.[9,10]

Moreover, many 7 T studies of the musculoskeletal system have been performed in cadavers, allowing imaging without motion artifacts even when using substantially longer acquisition times than in vivo examinations, and making it possible to overcome some of the mentioned problems in a study setting.[11,12]

With the advent of newer-generation 7 T scanners, commercially available extremity coils, and substantial improvements in artifact reduction, 7 T MRI has received increased attention,[13] so that we are now at the verge of a new paradigm in musculoskeletal imaging–clinical ultra-high-resolution MRI (Fig. 1).

Important questions now include how transformative clinical 7 T MRI will be and what the current state of 7 T MRI for the musculoskeletal system is. Unlike clinical MRI at 3 T field strength, 7 T MRI is not yet available for the entire musculoskeletal system. However, it has become evident that 7 T MRI can add value beyond the possibilities of lower field strengths for specific clinical questions.

Clinical MRI at 7 T and above has been previously reviewed with various levels of detail.[13–16] This review describes current state-of-the-art musculoskeletal 7 T MRI, addresses technological challenges and how to overcome them, and looks ahead at future developments. Increased spatial resolution is only a secondary goal that needs to translate into increased diagnostic accuracy. Therefore, we first discuss an important question from the clinical viewpoint: what are possible clinical use cases for musculoskeletal 7 T MRI with special attention to areas and indications where a better spatial resolution brings additional benefit for patient care and treating physicians?

## CLINICAL USE CASES FOR 7 T MRI

The joint most commonly evaluated with MRI is the knee: non-contrast 1.5 T and 3 T MRI have replaced diagnostic knee arthroscopy, which was still performed in large numbers at the beginning of this century in patients with unclear symptoms.[17] Magnetic resonance images acquired at 1.5 T or 3 T allow the radiologist to visualize internal derangements of the knee in a similar way as is possible during open surgery or even autopsy.[18]

Ex vivo histological studies and magnified views from arthroscopy allowed us to learn about the microanatomical structure of the menisci and the articular cartilage. However, current clinical MRI techniques

**FIGURE 1.** 7 T MRI knee protocol with turbo spin echo (TSE) sequences at the authors' institution. Although at lower field strength, TSE sequences are the mainstay of musculoskeletal MRI; at 7 T MRI, severe chemical shift artifacts and signal intensity inhomogeneities needed to be overcome for implementing TSE sequences. A, Coronal T1 sequence, (B) coronal proton density (PD) fat-saturated (fs) sequence, (C) sagittal PD fs sequence, and (D) axial PD fs sequence. Note that the small cartilage delamination (B) and superficial defects (C) of the femoral cartilage (arrowheads in inserts) are well depicted on high-resolution 7 T MRIs.

fail to provide an equally reliable depiction of the musculoskeletal anatomy in vivo at the same resolution.

Computed tomography and MR arthrography have been useful for a more accurate assessment of some internal derangement of the joints. However, they are invasive through the need for a direct injection of contrast agent into the joint under fluoroscopic or ultrasound guidance. With state-of-the-art 7 T MRI, it is possible to substantially increase spatial resolution, which helps detect small meniscal tears and delamination of the articular cartilage even in noncontrast studies (Fig. 1).

Dual-echo steady-state imaging at 7 T visualizes the meniscal and chondral calcifications in patients with calcium pyrophosphate deposition disease much better than at lower field strength and even more accurately than computed tomography.[19]

With ultra-high-field MRI, we can not only depict classic meniscal tears but also better assess the attachment of the medial meniscus to the posterior joint capsule. Meniscal ramp lesions may be missed in standard MRI and only intraoperatively recognized during anterior cruciate ligament (ACL) replacement surgery when the surgeon inspects the knee joint and tests the meniscus with a probe. Accurate preoperative identification of meniscal ramp lesions can change the treatment strategy.[20]

Magnetic resonance imaging of the knee in the preoperative situation or clinically suspected ACL tears are good examples of the potential of 7 T MRI for use in a specific clinical setting. Other possible scenarios for using 7 T MRI are preoperative evaluation and postsurgical follow-up of patients with indications for cartilage repair surgery, as high-resolution MRI of cartilage layers allows for better planning of the procedure and improves the quality control during the follow-up.[21]

Not every patient referred to knee MRI will need to undergo ultra-high-field MRI, but 7 T MRI will enhance our insight into anatomy and pathology in a subset of patients. Several ultra-high-resolution knee MRI studies are currently ongoing in our institutions, and in the next couple of years, we will have additional data regarding the differentiation of clinical use cases where 7 T MRI can offer a significant benefit and those where MRI at lower field strengths is sufficient.

Apart from the knee joint, possible use cases for musculoskeletal 7 T MRI will also emerge for other anatomical areas, such as ultra-high-resolution nerve imaging, the detection of cartilage delamination of the hip joint, or the improved depiction of osteochondral lesions of the ankle.[22,23]

Recent advances in metal-artifact reduction at ultra-high-field strength have also made it possible to reduce peri-implant signal voids and geometric distortions in the presence of metal with a combination of increased receive bandwidth, view-angle tilting, as well as slice-encoding for metal artifact correction.[24] The extent of metal artifacts is directly proportional to the field strength.[25] Therefore, metal artifact techniques at 7 T MRI will help obtain a homogeneous signal intensity in patients

**TABLE 1.** Comparative Relaxation Times at Magnetic Field Strengths of 3 T and 7 T*

| Tissue | T1, ms 3 T | T1, ms 7 T | T1 Ratio (7 T/3 T) | T2, ms 3 T | T2, ms 7 T | T2 Ratio (7 T/3 T) |
|---|---|---|---|---|---|---|
| Patellar cartilage | 1016 | 1568 | 1.54 | 39 | 32 | 0.82 |
| Subcutaneous fat | 404 | 583 | 1.44 | 48 | 46 | 0.96 |
| Femoral bone marrow | 381 | 549 | 1.44 | 52 | 47 | 0.90 |
| Lateral gastrocnemius muscle | 1256 | 1553 | 1.24 | 29 | 23 | 0.79 |
| Synovial fluid | 2565 | 4813 | 1.87 | 653 | 325 | 0.50 |

*Adapted from Jordan et al.[32]

undergoing 7 T MRI, for example, after ACL or tendon reconstructions. Typically, advanced acceleration techniques are required to attain clinically feasible scan times, for example, compressed sensing.[26]

Interestingly, although in the transition from 1.5 T to 3 T, the higher field strength was often used to speed up the image acquisition, scan-time reductions compared with 3 T MRI do not seem to have a high priority in current 7 T MRI. On the one hand, this is due to additional efforts required to mitigate image artifacts. On the other hand, the advent of ever-faster image acquisitions at lower field strengths,

for example, enabled by deep learning image reconstruction algorithms, has reduced the need to invest the higher SNR at 7 T for faster imaging.[27,28] Thus, 7 T MRI may mainly be attractive for its increased spatial resolution in clinical musculoskeletal imaging.

The increased SNR at 7 T may also enable potential applications beyond proton imaging: several groups have investigated the musculoskeletal system using 7 T sodium MRI, for instance, by detecting low-grade cartilage lesions or assessing cartilage stiffness in the knee.[29,30] 7 T was also used for phosphorus MR spectroscopy in skeletal muscle,[31] but the technique is experimental. In this review, we will focus on musculoskeletal [1]H 7 T MRI and its applications for clinical imaging that have substantially broadened the appeal of 7 T MRI in recent years.

## TECHNOLOGICAL CHALLENGES AND IMAGE OPTIMIZATION

### Relaxation Times

The 7 T longitudinal magnetization relaxation times (T1) of musculoskeletal tissues were reported to be moderately longer (20% to 60%) than corresponding T1 times at 3 T, with a particularly large increase in synovial fluid,[32] as shown in Table 1. The relaxation times and relative changes of the synovial fluid and other fluids strongly depend on macromolecular content and viscosity.[33–36] Interestingly, an opposite trend for hip cartilage T1 values, assessed with the dual flip-angle
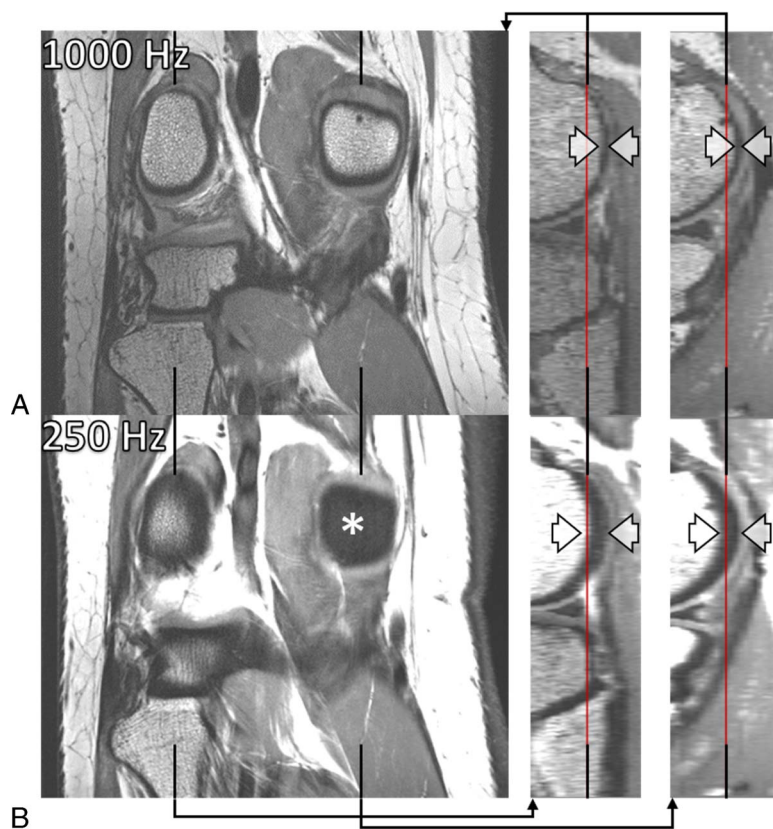


**FIGURE 2.** 7 T spin echo MRI with matched excitation and refocusing RF bandwidths showing coronal PD-weighted 2D TSE images of a right knee (on the left) and sagittal reformations through the lateral (in the middle) and the medial (on the right) femoral condyles. The 1 mm coronal images were acquired without gaps and with RF bandwidths of 1000 Hz (A) and 250 Hz (B) of the excitation (90 degrees) and refocusing (130 degrees) pulses, respectively, and with identical RF pulse durations in A and B. The lower RF bandwidth in B resulted in an increased through-slice (anterior-posterior direction) chemical-shift displacement of bone marrow and adipose tissue, as indicated by the caliper arrows. The asterisk (*) in B highlights a corresponding artifactual absence of signal in the coronal image. Also note the higher overall signal and the blurrier image appearance in B due to a less sharp definition of the 2D slice profile associated with the lower RF bandwidth. The phase- and frequency-encoding directions were right-left and superior-inferior, respectively.
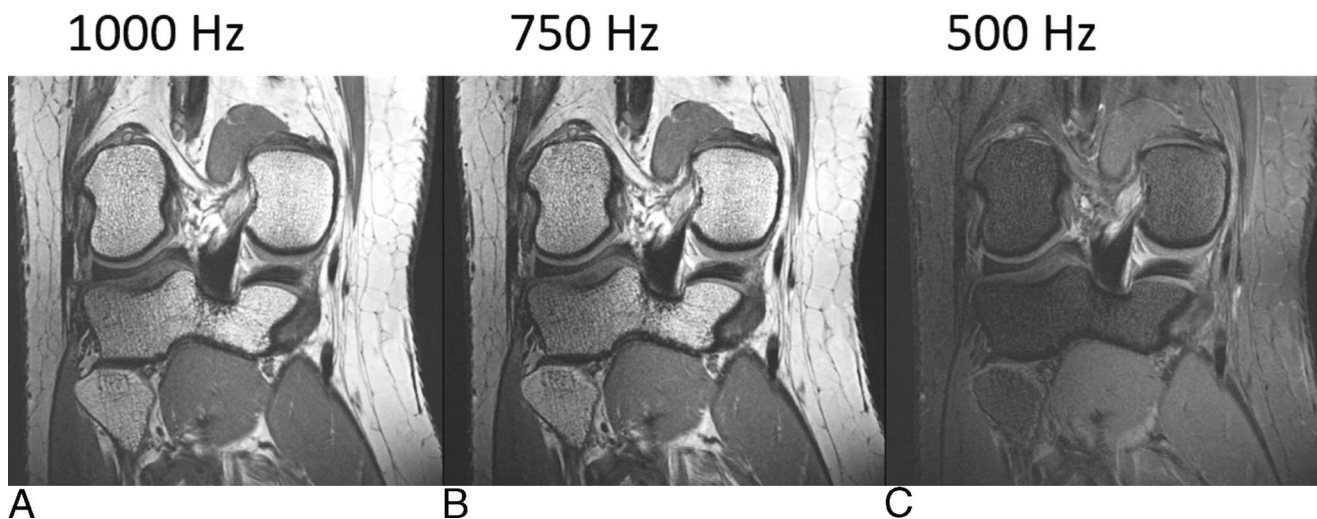
**FIGURE 3.** 7 T spin echo MRI with unmatched excitation and refocusing RF bandwidths using coronal PD-weighted 2D TSE images of a right knee acquired with identical parameters, except for the nominal RF bandwidth of the refocusing RF pulses (130 degrees), which was set to 1000, 750, and 500 Hz in A, B, and C, respectively. The 90-degree RF excitation pulse bandwidth was 1000 Hz. Estimated specific absorption rate values, SAR, were 0.26, 0.20, and 0.16 W/kg, respectively. The decreasing overlap of the slices with excited and refocused fat protons decreased fat-signal intensity from A to C. A moderate mismatch in B allowed a significant SAR reduction with a fat-signal loss that may be tolerable in many applications while still producing sufficiently crisp images due to the slice profile being dominated by the higher-bandwidth excitation pulse. A sufficiently large mismatch, as in C can provide fat-signal suppression without increased SAR.

method, was also published.[21] Increased T1 times may result in longer scan times compared with 3 T examinations; however, so far such differences are masked in most situations by different choice of acceleration factors and by specific absorption rate (SAR) limits at 7 T.

In contrast, the 7 T transverse magnetization relaxation times (T2) were only slightly shorter (4% to 21%) than corresponding 3 T values (Table 1), with the largest reduction in synovial fluid.[32] Nonsignificant T2 value differences were reported for hip cartilage[37] and a small to moderate reduction (5% to 32%) of T2 values in knee cartilage.[38]

The 7 T T2* times in retropatellar and hip cartilage were reported to be moderately shorter (12% to 36%) than the analogous 3 T values,[21,37] whereas more strongly reduced values (by 50%) were observed in UTE measurements of trabecular bone.[39] The shorter T2* times allow a shortening of experimental echo times (TE; and, thus, rep-

etition times, TR) in 7 T susceptibility-weighted and functional brain imaging protocols, where longer than minimum echo times are typically used. Adaptation of spin echo sequences to the changed relaxation times is described later.

## Chemical Shift

Hydrogen frequency differences caused by different degrees of chemical shielding linearly increase with magnetic field strength. The difference between the water resonance and the most prominent methylene resonance in fatty tissue and bone marrow increases from approximately 224 Hz at 1.5 T, to 448 Hz at 3 T, and 1045 Hz at 7 T.[40]

Thus, in the absence of a spatial field gradient, the bandwidth of a radiofrequency pulse, for example, a nonselective magnetization preparation pulse, should reach more than 1 kHz to affect fat and water
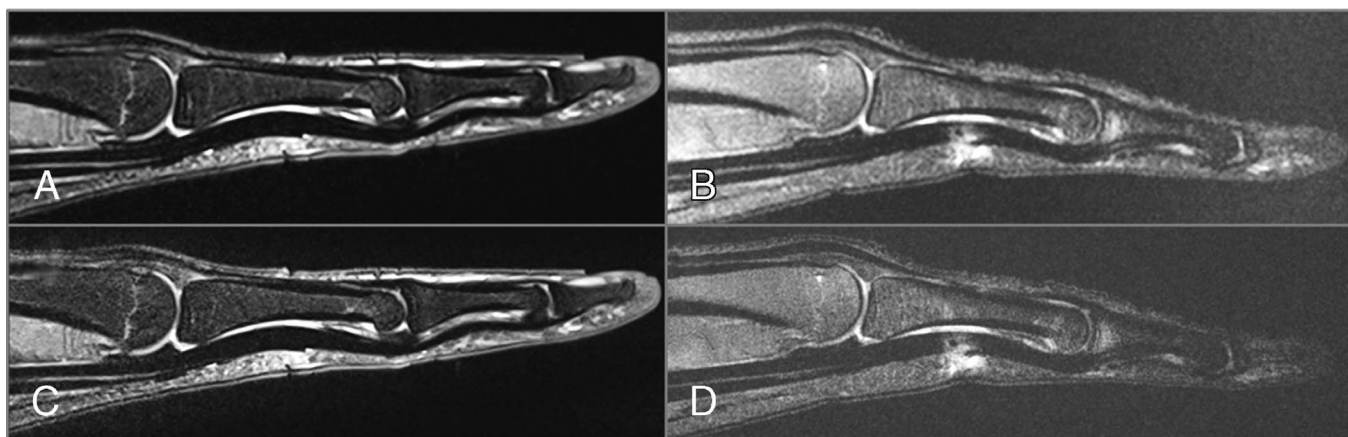


**FIGURE 4.** Intermediate weighted, fat-saturated sagittal finger MRI with identical TR and TE, acquired with a dedicated signal-receive hand coil at a field strength of 3 T (A and C) and a transmit-receive knee coil at 7 T (B and D) as off-label use. Acquisition parameters (A–D): TR, 3000 milliseconds; TE, 44 milliseconds; slice thickness, 2 mm; number of averages, 2. In-plane voxel dimensions: 0.19 mm² (A and B), 0.06 mm² (C and D); acquisition time: 2:26 minutes (A and B), 4:50 minutes (C and D); receive bandwidth: 116 kHz (A and B), 274 kHz (B and D); acquisition time: 2:26 minutes (A and B), 4:50 minutes (C and D). Note the lower signal-to-noise ratio of the 7 T MRIs despite the higher field strength. However, the receive bandwidths would not necessarily have had to be adapted for these fat-saturated images, and the TR should be longer at 7 T for comparable image quality.
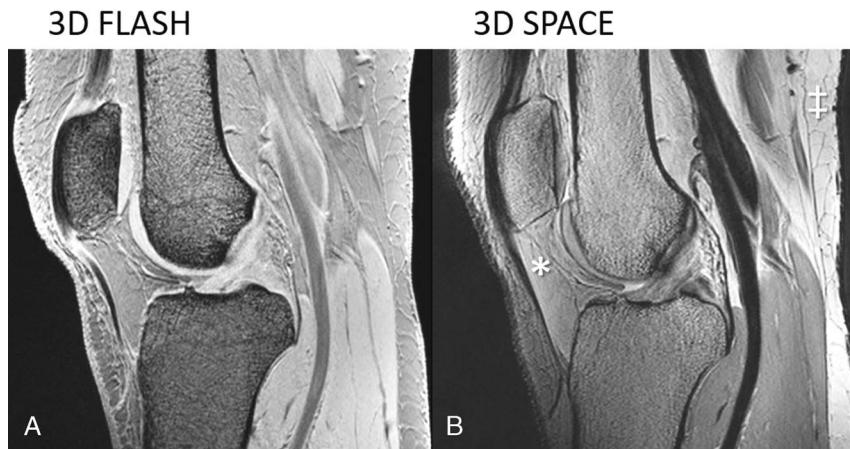
## 3D FLASH

## 3D SPACE



**FIGURE 5.** Sagittal 3D spoiled gradient echo 7 T MRI using (A) (FLASH; TR, TE, flip angle = 17.2 milliseconds, 2.04 milliseconds, 10 degrees) and sagittal turbo spin echo images (B) (SPACE; TR, $TE_{eff}$, flip angle, echo-train-length = 1500 milliseconds, 42 milliseconds, 120 degrees, 43) of the knee without fat-signal suppression. The TE in A corresponds to the second in-phase echo time. Note the dark appearance of bone marrow and fat in the gradient echo image and the inhomogeneous signal brightness in the turbo spin echo image (eg, relatively dark Hoffa's pad [*] versus bright posterior subcutaneous fat [‡]).

protons equally. If the pulse is applied with the same frequency as the water frequency, a bandwidth of even more than 2 kHz would seem desirable. However, higher RF bandwidths come at the cost of increased energy deposition and SAR.

In contrast, a low-SAR 2D or slab-selective RF pulse, which is simultaneously applied with a spatial field-gradient, most often affects fat as well as water protons; however, they are located in different slices within the body that are separated by a distance, $d$[5]:

$$d = \text{slice thickness} \times \frac{1045 \text{ Hz}}{\text{bandwidth}_{RF}}.$$

Thus, the fat and water structures that are conjointly imaged in a non–fat-suppressed 2D image actually stem from different slices. For example, RF pulses with a bandwidth of 250 Hz excite fat and water protons separated by 4 slice thicknesses at 7 T. This can result in images that are hard to interpret (Fig. 2).[5] For the same RF pulses at 1.5 T, the fat and water slices would only be separated by about a single slice thickness, which would often not be disturbing. The choice of differing, "unmatched" RF bandwidths for excitation and refocusing pulses,[5] with so-called

gradient reversal[41,42] at the extreme end, can provide a varying degree of fat saturation (Fig. 3), at the cost of some reduction of the water signal, in particular in areas of B0 inhomogeneity. An alternative low-SAR fat saturation approach that leverages parallel acceleration techniques has been suggested and verified in echo planar head imaging.[43]

### Static Field (B₀) Variations

Magnetic field strength and, thus, [1]H Larmor frequency differences between materials of different magnetic susceptibility linearly scale with the field strength, providing the well-known advantages[44] and challenges,[45] for example, for functional and susceptibility-weighted brain imaging at 7 T.[46] In the knee, this may contribute to the high sensitivity, with which 7 T MRI can detect calcified depositions in cartilage and menisci[19] and would likely help to increase the sensitivity in phase and susceptibility-weighted imaging[47] or T2* mapping[48] at 7 T. Homogenization of the magnetic field before acquisition and off-center imaging,[49] however, remains a challenge[50,51] that keeps being tackled most dynamically for head imaging.[52–54] Metal-induced susceptibility artifacts are particularly large at 7 T compared with those at lower field strength.[55,56]
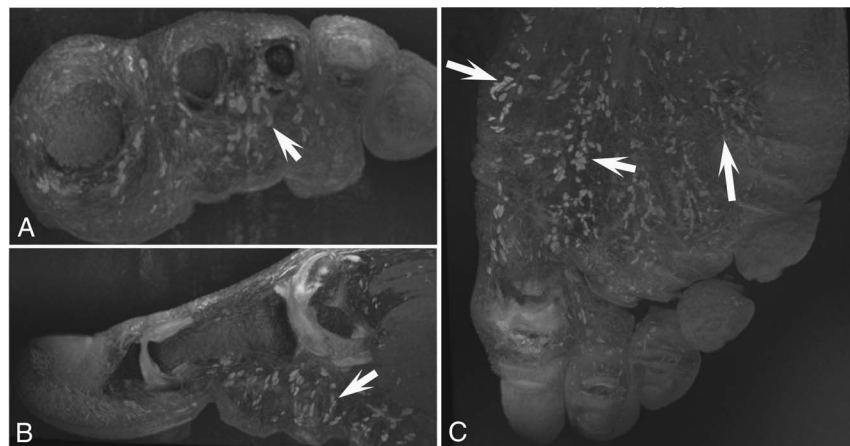


**FIGURE 6.** 7 T MRI of the left forefoot with transverse (A), sagittal (B), and coronal (C) 3D DESS reconstructions with partial maximum intensity projection in a 34-year-old asymptomatic male volunteer, demonstrating numerous Pacinian corpuscles (hyperintense ovoid nodules of 1–4 mm size in the plantar subcutaneous fat [arrows] and interdigitally arranged in chain-like formations), which are sensory receptors for vibration and deep pressure.

## Coils, Radiofrequency, B1, and SAR

Most local 7 T RF antennas are transmit and receive antennas, that is, smaller body parts are exposed to higher radiowave irradiation than in corresponding examinations at lower field strength that use a body transmit coil. CE-marked and FDA-cleared clinical ^{1}H hydrogen musculoskeletal imaging at 7 T is limited to the knee at the time of writing.

Some experimental coils have been successfully shown to allow imaging of various parts of the human musculoskeletal system in vivo, for example.[9,57–65] However, homogeneity of B1, signal intensity, and image contrast over larger volumes have proven to be goals that are not easy to reach, even in a volume as small as a human knee.

The scarcity of clinically approved, dedicated musculoskeletal coils that can homogeneously transmit ^{1}H radio waves into larger anatomical volumes without exceeding safety-relevant restrictions on local amplitudes, as well as receive the corresponding signals with homogeneous intensity may be one of the biggest roadblocks for a more common clinical use of 7 T systems (Fig. 4). Regulatory-cleared parallel-transmit systems[66,67] will be required to solve this issue. Promising steps toward a 7 T parallel-transmit body coil were recently reported.[68] Post–data acquisition attempts to homogenize signal intensity seem moderately successful.[69]

## Two-Dimensional Spin Echo MRI

Considering the role of 2D fast or turbo spin echo sequences in musculoskeletal imaging at lower field strengths,[70–72] their performance must be the first checkpoint when migrating from 3 T to 7 T.[7,73,74] A multiplication of TR and TE times by factors of 1.3 and 0.9, respectively, may be a reasonable first estimation based on the reported relaxation times.

Because of SAR limitations, it might often be necessary to reduce the number of acquired slices, the flip angle of the refocusing pulses, the length of the echo train, or to increase the repetition times and/or the number of concatenations.[75]

The use of low-SAR pulses may help a long way with obtaining high-resolution, fat-signal saturated images from a sufficiently large number of slices. However, this often will require RF bandwidths that are too low to acquire corresponding high-quality images without fat-signal suppression. There, the problems detailed under "chemical shift" and illustrated in Fig. 2 need to be solved.[5]

A more general report on how to mitigate 7 T image artifacts has been published, allowing to incorporate musculoskeletal 7 T MRI in the clinical workflow.[6]



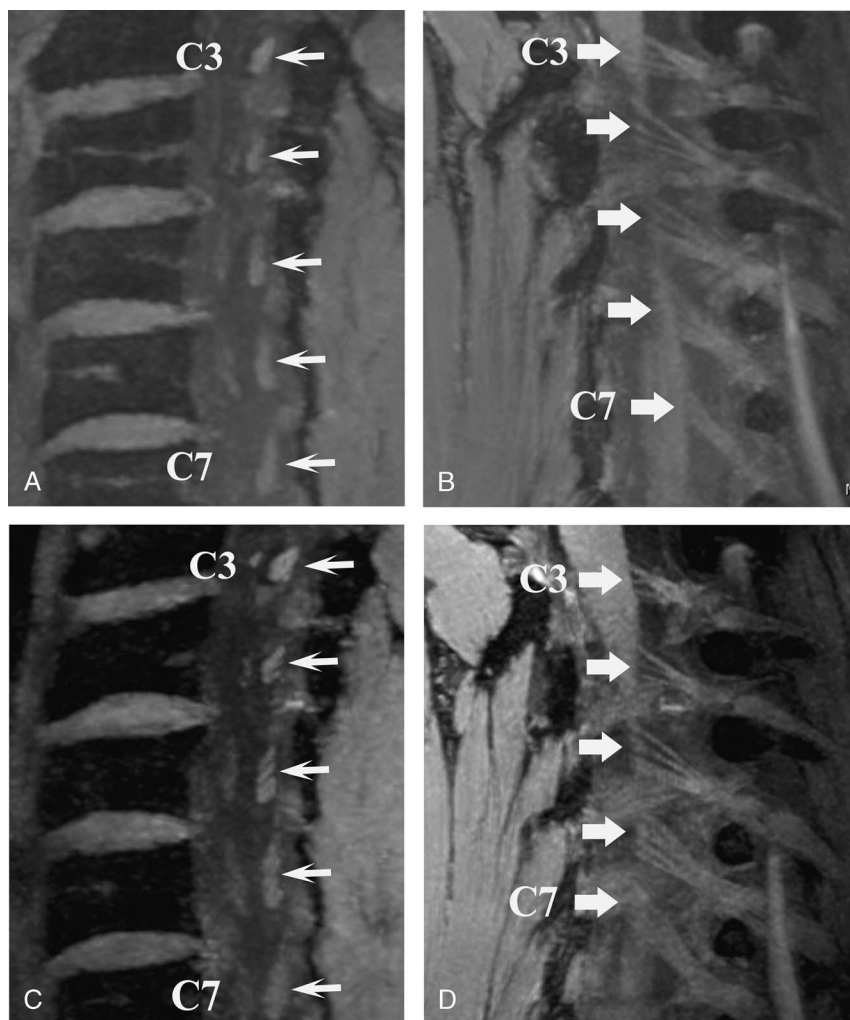**FIGURE 7.** 3D dual-echo steady-state (DESS) MRI of the cervical spine in a 34-year-old male healthy volunteer. Sagittal oblique reconstructions as a 5-mm maximal intensity projection visualizing the left posterior intraspinal nerve rootlets (arrows) of nerve roots C3–C7. A and B, 3 T MRI and (C and D) 7 T MRI. Note the higher contrast and higher number of rootlets that were identified at 7 T.

## Three-Dimensional MRI

A multitude of gradient echo–based sequences[75] and variable flip-angle turbo spin echo pulse sequences are available for 3-dimensional (3D) MRI at 7 T,[74,75] as shown in Figure 5. In comparison with corresponding acquisitions at lower field strengths, some salient points to note are as follows: (1) the B1 inhomogeneity and penetration depth issues are—in the authors' experience—most prominent for current 2D spin echo > 3D spin echo > 3D gradient echo–based imaging,[76] hypothetically in parallel with the number of high flip-angle RF pulses that need to be applied, (2) bone marrow seems remarkably dark in gradient echo–based images, even without fat-signal saturation, presumably because of short T2* times. In slab-selective 3D acquisitions, the previously discussed through-slice chemical-shift artifacts correspond to "through-slab" chemical-shift artifacts that can be observed in a few start and end slices, whereas in the central slices and in acquisition with nonselective high-bandwidth RF pulses, fat and water are consistently located in space along the 2 phase-encoding directions. This leaves only the "traditional" chemical-shift displacement along the frequency-encoding direction to be dealt with by appropriate adjustment of the receive bandwidth.

## CLINICAL IMPLEMENTATION

Although brain imaging is clinically implemented to a larger extent, musculoskeletal imaging at 7 T is less well developed. Similar to the early clinical implementation of 3 T, this is due partly to the limited commercial availability of 7 T array coils for musculoskeletal applications and the lack of radiofrequency hardware, well-matured imaging sequences, and evaluation software. However, promising studies were published during the last decade on musculoskeletal clinical applications and dedicated extremity coils,[48,60] and self-built coils have increasingly been constructed.[77–79]

Most importantly, the higher spatial resolution at 7 T helps the visualization of anatomical details and subtle lesions without the use of contrast agents, as has been demonstrated for knee,[73,80] foot muscles,[81] peripheral nerves, mechanoreceptors[82] (Fig. 6), and vessels of the upper extremity.[83,84]

In a study performed in our department, dual-echo steady-state MRI (DESS) at 3 T and at 7 T enabled noninvasive visualization of the microanatomy of the nerve rootlets that merge to form the cervical spinal nerve roots, with the higher field strength allowing identification of a larger number of cervical nerve rootlets[22] (Fig. 7).

Furthermore, cartilage, menisci, tendons, ligaments, and bones can possibly be better visualized with ultra-high-field MRI, allowing the detection of pathologies of these structures at an earlier stage and offering an opportunity for early interventions[19] (Fig. 8).

However, there is still a strong need to evaluate whether these advances provide additional benefits for patients in clinical settings compared with lower field strengths. It should also be considered that a 7 T MR system is associated with increased requirements for installation, operation, and maintenance. The results so far suggest that 7 T can be a valuable complementary tool to imaging at lower field strengths.
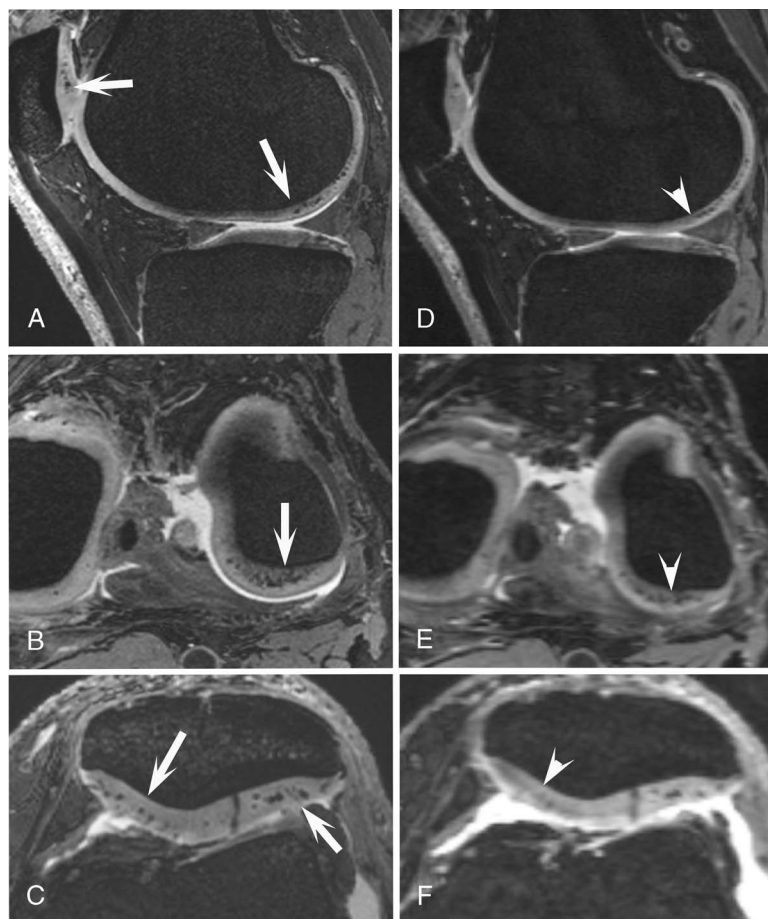


**FIGURE 8.** Spatially matched 3D dual-echo steady-state (DESS) images of a 66-year-old man. 7 T MRI (A–C) and 3 T MRI (D–F) of the left knee. At 7 T, the hypointense calcium crystal deposits in the femorotibial and patellar cartilage are clearly and sharply visible (arrows), whereas at 3 T MRI, these are much less visible, even without equivalent signal change (arrowheads).
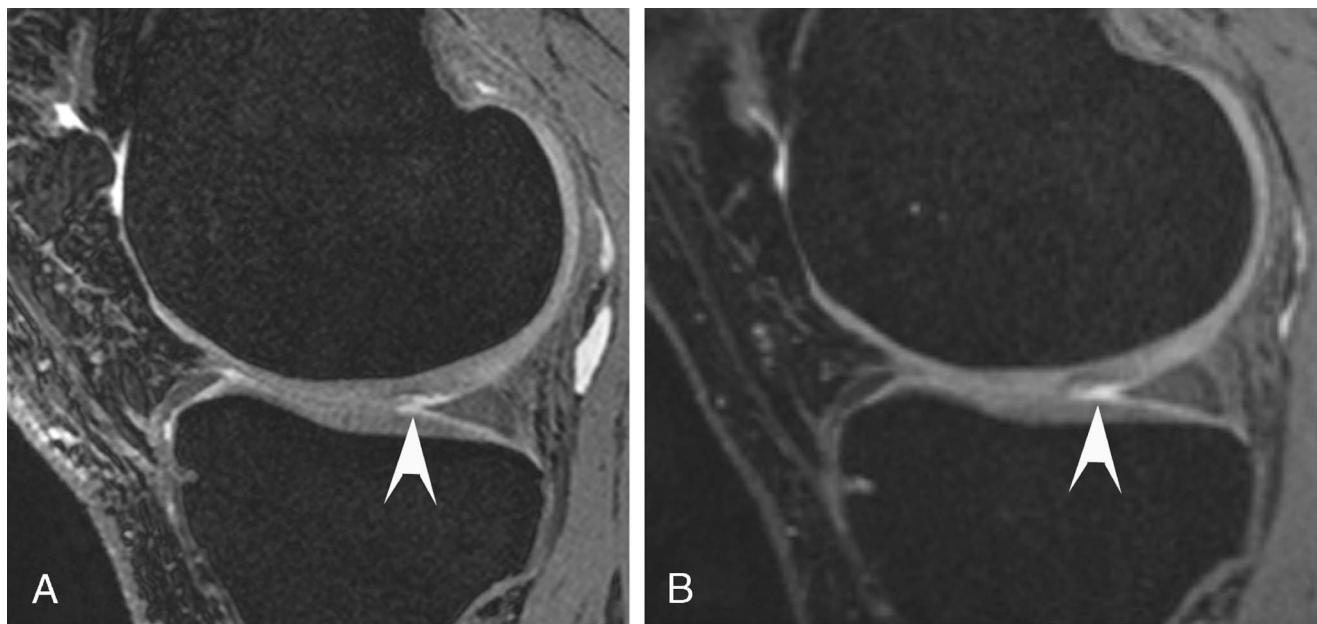
**FIGURE 9.** Sagittal 3D dual-echo steady-state (DESS) 7 T MRI (A) of an asymptomatic 43-year-old amateur athlete depicting delamination (arrowhead) of the femoral cartilage in the medial compartment of the knee, and corresponding sagittal 3 T DESS MRI (B), where the cartilage defect is less well defined (arrowhead).

Potential advantages and uses of ultra-high-field MRI in clinical routine are summarized later for selected target tissues.

## Articular Cartilage

Using dedicated coils and optimized protocols, 7 T MRI can visualize exquisite articular cartilage detail and subtle abnormalities, such as low-grade damage, and provide information about early structural changes, which are not readily seen with conventional MRI (Fig. 9). A systematic 7 T MRI evaluation of T2 relaxation times as a marker for cartilage integrity and collagen composition showed for the first time significant in vivo differences between the articular cartilage of the knee and ankle, confirming results of preceding biochemical and biomechanical studies.[85]

Surgical options for repairing damaged cartilage include microfracturing, osteochondral graft transplantation, autologous chondrocyte implantation, and juvenile cartilage cell implantation.[86] Imaging-based monitoring after surgery is a desirable tool to evaluate the success of therapy and compare outcomes so that evidence-based treatment decisions can be made.

To this end, Chang et al[87] quantified cartilage thickness and T2 values with 7 T MRI in 11 patients with cartilage repair and 11 healthy controls. They found thickness and T2 differences in the repair tissue compared with adjacent native cartilage and compared with cartilage from healthy subjects. They also described that the native cartilage adjacent to the repair tissue had normal thickness but lower T2 values than the cartilage of healthy control subjects and discussed whether that indicated a normal postoperative state due to lower water content/higher compressibility or early degeneration.[87]

Interestingly, similar results were shown for the ankle in a 7 T MRI study that quantified and compared T2 values of native tibiotalar cartilage and cartilage repair tissue in patients treated with a juvenile particulate allograft for osteochondral lesions of the talus.[88]

Lazik-Palm et al[21] focused on the morphology and quantitative analysis of cartilage in patients undergoing hip cartilage transplantation. They investigated 9 patients with a history of autologous acetabular cartilage transplantation with 7 T and 3 T MRI and compared the images regarding image quality, assessability of cartilage structures, and CNR among articular cartilage, joint fluid, and subchondral bone. They also measured the relaxation times of the transplanted acetabular and reference regions. 7 T MRI was superior to 3 T MRI regarding image quality, assessment of cartilage transplants, and contrast, whereas T2 relaxation times were longer at 7 T than 3 T but without statistical significance.[21]

## Meniscus

Chang et al[89] compared the dominant knee of asymptomatic dancers with nonathletic women at 7 T MRI and found no cartilage damage but occult medial meniscal lesions. Because this has been described in early osteoarthritis, they concluded that 7 T MRI could indicate preventive action to maintain long-term knee health in dancers.[89]

In a recent study, 41 patients with suspected meniscal damage or mild osteoarthritis were evaluated at both 7 T and 3 T MRI with an imaging protocol that consisted of PD-weighted imaging with nearly identical imaging acquisition times but more than doubled spatial resolution at 7 T MRI.[90] Three readers analyzed the images according to a modified whole-organ MRI score of the knee in osteoarthritis and the score of the International Cartilage Repair Society. The most important finding of this study was that in the 12 patients who underwent arthroscopy, the mean 7 T MRI cartilage and meniscus scores of each knee were significantly closer to the arthroscopy scores than the 3 T MRI scores. The authors also used a mixed model analysis of all 41 patients (with and without arthroscopy) and found significantly higher scores for cartilage and meniscal damage at 7 T than at 3 T MRI. The authors concluded that 7 T MRI diagnosed low-grade cartilage and meniscal damage with significantly higher accuracy.

To evaluate the healing process after meniscal suturing, Stelzeneder et al[91] evaluated meniscal tissue of 11 patients with 7 T MRI using sagittal T2 mapping at 6 and 12 months to determine T2 values of the red and white zones of each medial and lateral meniscus compared with healthy subjects. They found a healing response 12 months after meniscal repair in the red zone of the lateral posterior horn, which had similar T2 values as healthy subjects, but not in the medial meniscus, which did not reach normal T2 values at the 12-month follow-up.[91]

## Bone Density and Microstructure

Ultra-high-field MRI technology may be helpful to depict bone microarchitecture allowing a detailed analysis of trabecular cancellous bone to gain insight into age- and disease-related structural changes that are useful for evaluating treatment efficacy and monitoring. Spin echo–based pulse sequences are more suitable for high-resolution trabecular bone imaging because they are less sensitive to undesired inhomogeneity of the magnetic field but tend to be associated with high power output.

Magland et al[92] introduced a modified, reduced SAR, 3D, fast spin echo pulse sequence specifically optimized for in vivo trabecular bone imaging of the distal tibia at 1.5 T, 3 T, and 7 T MRI, demonstrating that a significant SAR reduction can be achieved with negligible SNR loss at 7 T. GRAPPA-based parallel imaging with an acceleration factor of 1.8 reduced the 7 T scan time from 13 minutes to 10.2 minutes.

Another study showed high reproducibility for 7 T MRI subregional trabecular bone microarchitecture measurements of the distal tibia scanned on the same day and different days.[93] Similar results were achieved in other feasibility studies at 7 T for imaging trabecular bone microarchitecture of the wrist[77] and knee.[94]

Today's experience suggests that 7 T MRI improves trabecular bone imaging by providing higher spatial resolution, efficient scan times, and sufficient SNR despite using parallel imaging.

Promising results show that 7 T MRI can detect microarchitectural deterioration in women with fragility fractures that bone mineral density measurements by dual-energy x-ray absorptiometry failed to expose.[95]

## Tendons

A 3D ultrashort time echo pulse sequence was used to compare 7 T and 3 T MRI for Achilles tendon evaluation in healthy volunteers and patients with chronic Achilles tendinopathy. Unexpectedly, the SNR was higher at 3 T than at 7 T, which the authors attributed to the differences in the noise profiles of the individual coils and more pronounced radial streak artifacts on the 7 T images. However, the CNR between tendons and calf muscles was almost twice as high on 7 T than 3 T MRIs.[96] The authors found regional differences in T2* values and differences between field strengths and between healthy and degenerated tendons, demonstrating a higher accuracy of T2* calculations with 7 T compared with 3 T MRI. They concluded that T2* could be a useful quantitative marker for the early detection of Achilles tendon tendinopathy and subclinical tendon damage, invisible to morphological imaging.[96]

Even greater difficulties need to be overcome for 7 T MRI of rotator cuff tendons. The feasibility of 7 T shoulder MRI with a diagnostic image quality was demonstrated by Lazik-Palm et al[49] using a C-shaped 8-channel transmit/receive coil, and a 7-channel receive coil; however, with inferior diagnostic accuracy compared with 3 T or 1.5 T studies. In their MRI protocols, short echo times (30–35 milliseconds) were chosen for the fat-saturated PD-weighted pulse sequence, prioritizing a higher SNR over a reduction of magic-angle effects, which may have led to an overcalling of supraspinatus tendinopathy.[49]

## Muscles

The higher spatial and temporal resolution of 7 T MRI can be beneficial for depicting muscle edema and the extent of fatty infiltration. For example, 2D chemical-shift imaging can differentiate and quantify extramyocellular and intramyocellular lipids,[97] which can be a marker of whole-body insulin sensitivity in diabetes mellitus.[98,99]

The higher SNR at 7 T can also benefit diffusion-tensor imaging (DTI) and enable more detailed studies of muscle-fiber architecture and, thus, provide a tool for investigating muscle tears, for example, in athletes. Giraudo et al[100] compared DTI metrics for calf muscles at 3 T with 7 T MRI and found a significant improvement of fiber tracking at the higher field strength. However, their results were heterogeneous, for example, the average 7 T fractional anisotropy (FA) was higher, and the 7 T mean diffusivity (MD) values were lower in the soleus muscle, but exactly opposite trends were measured for the anterior tibial muscle. The authors discuss that this heterogeneity supports the assumption that the use of 7 T is beneficial for studying certain areas.[100,101] Finally, they concluded an overall equivalence of the 2 field strengths except for the superior performance of 7 T for the number of fibers tracked in the entire calf and increased FA of the lateral gastrocnemius at 3 T. However, it should be noted that muscle DTI is still primarily used for research purposes and not applied in everyday clinical practice.

The muscle-tissue perfusion and, associated with it, the oxygen supply to the tissue is important for assessing muscle function, which is of clinical interest in patients with peripheral arterial disease.[102] The perfusion can be quantified by arterial spin labeling (ASL) without the application of gadolinium, but both low SNR and signal decay during inflow time due to T1 relaxation limit ASL measurements. In a feasibility study, Schewzow et al[103] measured reliable quantitative perfusion values of the calf muscles before, during, and after plantar flexion in healthy subjects using pulsed ASL. They optimized the data acquisition for high SNR and enough temporal resolution to detect significant perfusion changes after exercise, thus representing the dynamics of muscle perfusion.

## Peripheral Nerves

High-resolution MRI of peripheral nerves offers a potential application for detecting and monitoring neuropathy, including inflammatory pathologies, traumatic peripheral nerve injury or nerve regeneration, and follow-up examination under therapy.

Recently, a 12-channel wrist coil and a triple-echo steady-state (TESS) sequence have been used to assess the number of axonal bundles (fascicles) in the median nerve and to determine the normative T2 values, which seem to be associated with pathophysiological nerve changes.[84] This study found higher T2 values for patients with idiopathic carpal tunnel syndrome (24.27 ± 0.97 milliseconds) than healthy volunteers (21.01 ± 0.65 milliseconds). The authors further could identify ultrastructural components of the relatively small median nerve due to the high resolution available at 7 T.[84]

Another study evaluated nerve imaging of the upper extremity at 7 T compared with 3 T.[83] The quantitative analyses showed almost twice as high SNR and CNR values at 7 T, which allowed high-resolution MRI with volume rendering and 3D depiction of the course of the forearm nerves.[83] The macrovascular and microvascular anatomy of the hand, forearm, and wrist were also clearly visualized using non–contrast-enhanced time-of-flight imaging.

## CONCLUSIONS

Musculoskeletal MRI at 7 T has received increased attention with the advent of newer-generation 7 T scanners, commercially available extremity coils, and substantial improvements in artifact reduction. We are now on the verge of clinical ultra-high-resolution MRI. Unlike the transition from 1.5 T to 3 T, where the higher field strength was often used to accelerate image acquisition, the higher field strength at 7 T is more commonly used for obtaining higher spatial resolution to visualization of small anatomical musculoskeletal structures and internal derangements of the joints. To achieve this goal, specific sequence improvements at 7 T must be implemented to mitigate various artifacts that have previously reduced the image quality at 7 T. Dedicated coils for specific anatomic regions are also required for clinical 7 T MRI of the knee joint and other musculoskeletal regions such as the foot and spine. Identifying and validating clinical use cases will help determine when MRI at lower field strength is sufficient and when 7 T MRI will add value.

# REFERENCES

1. Khodarahmi I, Fritz J. The value of 3 Tesla field strength for musculoskeletal magnetic resonance imaging. *Invest Radiol*. 2021;56:749–763.

2. Schick F, Pieper CC, Kupczyk P, et al. 1.5 vs 3 Tesla magnetic resonance imaging: a review of favorite clinical applications for both field strengths—Part 1. *Invest Radiol*. 2021;56:680–691.

3. Yacoub E, Shmuel A, Pfeuffer J, et al. Imaging brain function in humans at 7 Tesla. *Magn Reson Med*. 2001;45:588–594.

4. Robitaille PM, Warner R, Jagadeesh J, et al. Design and assembly of an 8 Tesla whole-body MR scanner. *J Comput Assist Tomogr*. 1999;23:808–820.

5. von Deuster C, Sommer S, Germann C, et al. Controlling through-slice chemical-shift artifacts for improved non-fat-suppressed musculoskeletal turbo-spin-echo magnetic resonance imaging at 7 T. *Invest Radiol*. 2021;56:545–552.

6. Fagan AJ, Welker KM, Amrami KK, et al. Image artifact management for clinical magnetic resonance imaging on a 7 T scanner using single-channel radiofrequency transmit mode. *Invest Radiol*. 2019;54:781–791.

7. Juras V, Welsch G, Bär P, et al. Comparison of 3T and 7T MRI clinical sequences for ankle imaging. *Eur J Radiol*. 2012;81:1846–1850.

8. Nöbauer-Huhmann IM, Pretterklieber M, Erhart J, et al. Anatomy and variants of the triangular fibrocartilage complex and its MR appearance at 3 and 7T. *Semin Musculoskelet Radiol*. 2012;16:93–103.

9. Chang G, Deniz CM, Honig S, et al. MRI of the hip at 7T: feasibility of bone microarchitecture, high-resolution cartilage, and clinical imaging. *J Magn Reson Imaging*. 2014;39:1384–1393.

10. Griffin LM, Honig S, Chen C, et al. 7T MRI of distal radius trabecular bone microarchitecture: how trabecular bone quality varies depending on distance from end-of-bone. *J Magn Reson Imaging*. 2017;45:872–878.

11. Van Sint Jan S, Rooze M, Van Audekerke J, et al. The insertion of the extensor digitorum tendon on the proximal phalanx. *J Hand Surg Am*. 1996;21:69–76.

12. Moon SM, Yoder JH, Wright AC, et al. Evaluation of intervertebral disc cartilaginous endplate structure using magnetic resonance imaging. *Eur Spine J*. 2013; 22:1820–1828.

13. Aringhieri G, Zampa V, Tosetti M. Musculoskeletal MRI at 7 T: do we need more or is it more than enough? *Eur Radiol Exp*. 2020;4:48.

14. Krug R, Stehling C, Kelley DA, et al. Imaging of the musculoskeletal system in vivo using ultra-high field magnetic resonance at 7 T. *Invest Radiol*. 2009;44: 613–618.

15. Trattnig S, Bogner W, Gruber S, et al. Clinical applications at ultrahigh field (7 T). Where does it make the difference? *NMR Biomed*. 2016;29:1316–1334.

16. Platt T, Ladd ME, Paech D. 7 Tesla and beyond: advanced methods and clinical applications in magnetic resonance imaging. *Invest Radiol*. 2021;56:705–725.

17. Smith L, Barratt A, Buchbinder R, et al. Trends in knee magnetic resonance imaging, arthroscopies and joint replacements in older Australians: still too much low-value care? *ANZ J Surg*. 2020;90:833–839.

18. Sutter R, Stoel BC, Buck FM, et al. Internal derangements of joints—past, present, and future. *Invest Radiol*. 2015;50:601–614.

19. Germann C, Galley J, Falkowski AL, et al. Ultra-high resolution 3D MRI for chondrocalcinosis detection in the knee—a prospective diagnostic accuracy study comparing 7-Tesla and 3-tesla MRI with CT. *Eur Radiol*. 2021;31: 9436–9445.

20. DePhillipo NN, Engebretsen L, LaPrade RF. Current trends among US surgeons in the identification, treatment, and time of repair for medial meniscal ramp lesions at the time of ACL surgery. *Orthop J Sports Med*. 2019; 7:2325967119882767.

21. Lazik-Palm A, Kraff O, Johst S, et al. Morphological and quantitative 7 T MRI of hip cartilage transplants in comparison to 3 T—initial experiences. *Invest Radiol*. 2016;51:552–559.

22. Galley J, Sutter R, Germann C, et al. High-resolution in vivo MR imaging of intraspinal cervical nerve rootlets at 3 and 7 Tesla. *Eur Radiol*. 2021;31: 4625–4633.

23. Rizzo R, Cristoforetti A, Marinetti A, et al. Quantitative MRI T2 mapping is able to assess tissue quality after reparative and regenerative treatments of osteochondral lesions of the talus. *J Magn Reson Imaging*. 2021;54:1572–1582.

24. Germann C, Falkowski AL, von Deuster C, et al. Basic and advanced metal-artifact reduction techniques at ultra-high field 7-T magnetic resonance imaging—phantom study investigating feasibility and efficacy. *Invest Radiol*. 2022;57:387–398.

25. Germann C, Nanz D, Sutter R. Magnetic resonance imaging around metal at 1.5 Tesla: techniques from basic to advanced and clinical impact. *Invest Radiol*. 2021;56:734–748.

26. Fritz J, Ahlawat S, Demehri S, et al. Compressed sensing SEMAC: 8-fold accelerated high resolution metal artifact reduction MRI of cobalt-chromium knee arthroplasty implants. *Invest Radiol*. 2016;51:666–676.

27. Fayad LM, Parekh VS, de Castro Luna R, et al. A deep learning system for synthetic knee magnetic resonance imaging: is artificial intelligence-based fat-suppressed imaging feasible? *Invest Radiol*. 2021;56:357–368.

28. Herrmann J, Koerzdoerfer G, Nickel D, et al. Feasibility and implementation of a deep learning MR reconstruction for TSE sequences in musculoskeletal imaging. *Diagnostics (Basel)*. 2021;11:1484.

29. Zbýň Š, Schreiner M, Juras V, et al. Assessment of low-grade focal cartilage lesions in the knee with sodium MRI at 7 T: reproducibility and short-term, 6-month follow-up data. *Invest Radiol*. 2020;55:430–437.

30. Brinkhof S, Froeling M, Janssen RPA, et al. Can sodium MRI be used as a method for mapping of cartilage stiffness? *MAGMA*. 2021;34:327–336.

31. Parasoglou P, Xia D, Chang G, et al. Dynamic three-dimensional imaging of phosphocreatine recovery kinetics in the human lower leg muscles at 3T and 7T: a preliminary study. *NMR Biomed*. 2013;26:348–356.

32. Jordan CD, Saranathan M, Bangerter NK, et al. Musculoskeletal MRI at 3.0 T and 7.0 T: a comparison of relaxation times and image contrast. *Eur J Radiol*. 2013;82:734–739.

33. Bagher-Ebadian H, Paudyal R, Nagaraja TN, et al. MRI estimation of gadolinium and albumin effects on water proton. *Neuroimage*. 2011;54 Suppl 1(suppl 1):S176–S179.

34. Stanisz GJ, Henkelman RM. Gd-DTPA relaxivity depends on macromolecular content. *Magn Reson Med*. 2000;44:665–667.

35. Taraban MB, Briggs KT, Yu YB. Magnetic resonance relaxometry for determination of protein concentration and aggregation. *Curr Protoc Protein Sci*. 2020;99:e102.

36. van Leeuwen FHP, Lena B, Zwanenburg JJM, et al. Detecting low blood concentrations in joints using T1 and T2 mapping at 1.5, 3, and 7 T: an in vitro study. *Eur Radiol Exp*. 2021;5:51.

37. Welsch GH, Apprich S, Zbyn S, et al. Biochemical (T2, T2* and magnetisation transfer ratio) MRI of knee cartilage: feasibility at ultra-high field (7T) compared with high field (3T) strength. *Eur Radiol*. 2011;21:1136–1143.

38. Juras V, Schreiner M, Laurent D, et al. The comparison of the performance of 3 T and 7 T T2 mapping for untreated low-grade cartilage lesions. *Magn Reson Imaging*. 2019;55:86–92.

39. Wurnig MC, Calcagni M, Kenkel D, et al. Characterization of trabecular bone density with ultra-short echo-time MRI at 1.5, 3.0 and 7.0T—comparison with micro-computed tomography. *NMR Biomed*. 2014;27:1159–1166.

40. Hood MN, Ho VB, Smirniotopoulos JG, et al. Chemical shift: the artifact and clinical tool revisited. *Radiographics*. 1999;19:357–371.

41. Park HW, Kim DJ, Cho ZH. Gradient reversal technique and its applications to chemical-shift-related NMR imaging. *Magn Reson Med*. 1987;4:526–536.

42. Wyss M, Manoliu A, Marcon M, et al. Clinical magnetic resonance imaging of the knee at 7 T: optimization of fat suppression. *Invest Radiol*. 2019;54:160–168.

43. Seginer A, Furman-Haran E, Goldberg I, et al. Reducing SAR in 7T brain fMRI by circumventing fat suppression while removing the lipid signal through a parallel acquisition approach. *Sci Rep*. 2021;11:15371.

44. van Lanen RHGJ, Colon AJ, Wiggins CJ, et al. Ultra-high field magnetic resonance imaging in human epilepsy: a systematic review. *Neuroimage Clin*. 2021;30:102602.

45. Dymerska B, Poser BA, Barth M, et al. A method for the dynamic correction of B0-related distortions in single-echo EPI at 7T. *Neuroimage*. 2018;168:321–331.

46. Uğurbil K. Imaging at ultrahigh magnetic fields: history, challenges, and solutions. *Neuroimage*. 2018;168:7–32.

47. Kolb A, Robinson S, Stelzeneder D, et al. Vessel architecture in human knee cartilage in children: an in vivo susceptibility-weighted imaging study at 7 T. *Eur Radiol*. 2018;28:3384–3392.

48. Zbýň Š, Santiago C, Johnson CP, et al. Compositional evaluation of lesion and parent bone in patients with juvenile osteochondritis dissecans of the knee using T2 * mapping. *J Orthop Res*. 2021;10.1002/jor.25187.

49. Lazik-Palm A, Kraff O, Rietsch SHG, et al. 7-T clinical MRI of the shoulder in patients with suspected lesions of the rotator cuff. *Eur Radiol Exp*. 2020;4:10.

50. Verma T, Cohen-Adad J. Effect of respiration on the B0 field in the human spinal cord at 3T. *Magn Reson Med*. 2014;72:1629–1636.

51. Winkler SA, Schmitt F, Landes H, et al. Gradient and shim technologies for ultra high field MRI. *Neuroimage*. 2018;168:59–70.

52. Hetherington HP, Moon CH, Schwerter M, et al. Dynamic B0 shimming for multiband imaging using high order spherical harmonic shims. *Magn Reson Med*. 2021;85:531–543.

53. Stockmann JP, Wald LL. In vivo B0 field shimming methods for MRI at 7 T. *Neuroimage*. 2018;168:71–87.

54. Stockmann JP, Arango NS, Witzel T, et al. A 31-channel integrated "AC/DC" B0 shim and radiofrequency receive array coil for improved 7T MRI. *Magn Reson Med*. 2022;87:1074–1092.

55. Chiba Y, Murakami H, Sasaki M, et al. Quantification of metal-induced susceptibility artifacts associated with ultrahigh-field magnetic resonance imaging of spinal implants. *JOR Spine*. 2019;2:e1064.

56. Spronk T, Kraff O, Kreutner J, et al. Development and evaluation of a numerical simulation approach to predict metal artifacts from passive implants in MRI. *MAGMA*. 2021.

57. Kraff O, Bitz AK, Dammann P, et al. An eight-channel transmit/receive multi-purpose coil for musculoskeletal MR imaging at 7 T. *Med Phys*. 2010;37:6368–6376.

58. Webb AG, Collins CM, Versluis MJ, et al. MRI and localized proton spectroscopy in human leg muscle at 7 tesla using longitudinal traveling waves. *Magn Reson Med*. 2010;63:297–302.

59. Nordmeyer-Massner JA, Wyss M, Andreisek G, et al. In vitro and in vivo comparison of wrist MR imaging at 3.0 and 7.0 tesla using a gradient echo sequence and identical eight-channel coil array designs. *J Magn Reson Imaging*. 2011;33:661–667.

60. Vossen M, Teeuwisse W, Reijnierse M, et al. A radiofrequency coil configuration for imaging the human vertebral column at 7 T. *J Magn Reson*. 2011;208:291–297.

61. Raghuraman S, Mueller MF, Zbýň Š, et al. 12-channel receive array with a volume transmit coil for hand/wrist imaging at 7 T. *J Magn Reson Imaging*. 2013;38:238–244.

62. Brown R, Deniz CM, Zhang B, et al. Design and application of combined 8-channel transmit and 10-channel receive arrays and radiofrequency shimming for 7-T shoulder magnetic resonance imaging. *Invest Radiol*. 2014;49:35–47.

63. Rietsch SHG, Pfaffenrot V, Bitz AK, et al. An 8-channel transceiver 7-channel receive RF coil setup for high SNR ultrahigh-field MRI of the shoulder at 7 T. *Med Phys*. 2017;44:6195–6208.

64. Barry RL, Vannesjo SJ, By S, et al. Spinal cord MRI at 7T. *Neuroimage*. 2018;168:437–451.

65. Rietsch SHG, Brunheim S, Orzada S, et al. Development and evaluation of a 16-channel receive-only RF coil to improve 7T ultra-high field body MRI with focus on the spine. *Magn Reson Med*. 2019;82:796–810.

66. Deniz CM. Parallel transmission for ultrahigh field MRI. *Top Magn Reson Imaging*. 2019;28:159–171.

67. Uğurbil K, Van de Moortele PF, Grant A, et al. Progress in imaging the human torso at the ultrahigh fields of 7 and 10.5 T. *Magn Reson Imaging Clin N Am*. 2021;29:e1–e19.

68. Fiedler TM, Orzada S, Flöser M, et al. Performance and safety assessment of an integrated transmit array for body imaging at 7 T under consideration of specific absorption rate, tissue temperature, and thermal dose. *NMR Biomed*. 2022;35:e4656.

69. Chebrolu VV, Kollasch PD, Deshpande V, et al. Uniform combined reconstruction of multichannel 7 T knee MRI receive coil data without the use of a reference scan. *J Magn Reson Imaging*. 2019;50:1534–1544.

70. Garwood ER, Recht MP, White LM. Advanced imaging techniques in the knee: benefits and limitations of new rapid acquisition strategies for routine knee MRI. *AJR Am J Roentgenol*. 2017;209:552–560.

71. Altahawi F, Pierce J, Aslan M, et al. 3D MRI of the knee. *Semin Musculoskelet Radiol*. 2021;25:455–467.

72. Kijowski R. 3D MRI of articular cartilage. *Semin Musculoskelet Radiol*. 2021;25:397–408.

73. Welsch GH, Juras V, Szomolanyi P, et al. Magnetic resonance imaging of the knee at 3 and 7 tesla: a comparison using dedicated multi-channel coils and optimised 2D and 3D protocols. *Eur Radiol*. 2012;22:1852–1859.

74. Springer E, Bohndorf K, Juras V, et al. Comparison of routine knee magnetic resonance imaging at 3 T and 7 T. *Invest Radiol*. 2017;52:42–54.

75. Stahl R, Krug R, Kelley DA, et al. Assessment of cartilage-dedicated sequences at ultra-high-field MRI: comparison of imaging performance and diagnostic confidence between 3.0 and 7.0 T with respect to osteoarthritis-induced changes at the knee joint. *Skeletal Radiol*. 2009;38:771–783.

76. Kraff O, Fischer A, Nagel AM, et al. MRI at 7 tesla and above: demonstrated and potential capabilities. *J Magn Reson Imaging*. 2015;41:13–33.

77. Chang G, Friedrich KM, Wang L, et al. MRI of the wrist at 7 tesla using an eight-channel array coil combined with parallel imaging: preliminary results. *J Magn Reson Imaging*. 2010;31:740–746.

78. Krug R, Larson PE, Wang C, et al. Ultrashort echo time MRI of cortical bone at 7 tesla field strength: a feasibility study. *J Magn Reson Imaging*. 2011;34:691–695.

79. Theysohn JM, Kraff O, Orzada S, et al. Bilateral hip imaging at 7 Tesla using a multi-channel transmit technology: initial results presenting anatomical detail in healthy volunteers and pathological changes in patients with avascular necrosis of the femoral head. *Skeletal Radiol*. 2013;42:1555–1563.

80. Kraff O, Theysohn JM, Maderwald S, et al. MRI of the knee at 7.0 Tesla. *Rofo*. 2007;179:1231–1235.

81. Franettovich Smith MM, Elliott JM, Al-Najjar A, et al. New insights into intrinsic foot muscle morphology and composition using ultra-high-field (7-Tesla) magnetic resonance imaging. *BMC Musculoskelet Disord*. 2021;22:97.

82. Germann C, Sutter R, Nanz D. Novel observations of Pacinian corpuscle distribution in the hands and feet based on high-resolution 7-T MRI in healthy volunteers. *Skeletal Radiol*. 2021;50:1249–1255.

83. Raval SB, Britton CA, Zhao T, et al. Ultra-high field upper extremity peripheral nerve and non-contrast enhanced vascular imaging. *PLoS One*. 2017;12:e0175629.

84. Riegler G, Drlicek G, Kronnerwetter C, et al. High-resolution axonal bundle (fascicle) assessment and triple-echo steady-state T2 mapping of the median nerve at 7 T: preliminary experience. *Invest Radiol*. 2016;51:529–535.

85. Juras V, Zbýň Š, Mlynarik V, et al. The compositional difference between ankle and knee cartilage demonstrated by T2 mapping at 7 Tesla MR. *Eur J Radiol*. 2016;85:771–777.

86. Trattnig S, Domayer S, Welsch GW, et al. MR imaging of cartilage and its repair in the knee—a review. *Eur Radiol*. 2009;19:1582–1594.

87. Chang G, Xia D, Sherman O, et al. High resolution morphologic imaging and T2 mapping of cartilage at 7 Tesla: comparison of cartilage repair patients and healthy controls. *MAGMA*. 2013;26:539–548.

88. Vira S, Ramme AJ, Chang G, et al. Juvenile particulate osteochondral allograft for treatment of osteochondral lesions of the talus: detection of altered repair tissue biochemical composition using 7 Tesla MRI and T2 mapping. *J Foot Ankle Surg*. 2017;56:26–29.

89. Chang G, Diamond M, Nevsky G, et al. Early knee changes in dancers identified by ultra-high-field 7 T MRI. *Scand J Med Sci Sports*. 2014;24:678–682.

90. Friebe B, Richter M, Penzlin S, et al. Assessment of low-grade meniscal and cartilage damage of the knee at 7 T: a comparison to 3 T imaging with arthroscopic correlation. *Invest Radiol*. 2018;53:390–396.

91. Stelzeneder B, Trabauer BM, Aldrian S, et al. Evaluation of meniscal tissue after meniscal repair using ultrahigh field MRI. *J Knee Surg*. 2021;34:1337–1348.

92. Magland JF, Rajapakse CS, Wright AC, et al. 3D fast spin echo with out-of-slab cancellation: a technique for high-resolution structural imaging of trabecular bone at 7 Tesla. *Magn Reson Med*. 2010;63:719–727.

93. Chang G, Wang L, Liang G, et al. Reproducibility of subregional trabecular bone micro-architectural measures derived from 7-Tesla magnetic resonance images. *MAGMA*. 2011;24:121–125.

94. Krug R, Carballido-Gamio J, Banerjee S, et al. In vivo bone and cartilage MRI using fully-balanced steady-state free-precession at 7 tesla. *Magn Reson Med*. 2007;58:1294–1298.

95. Alizai H, Chang G, Regatte RR. MRI of the musculoskeletal system: advanced applications using high and ultrahigh field MRI. *Semin Musculoskelet Radiol*. 2015;19:363–374.

96. Juras V, Zbyn S, Pressl C, et al. Regional variations of $T_2^*$ in healthy and pathologic achilles tendon in vivo at 7 Tesla: preliminary results. *Magn Reson Med*. 2012;68:1607–1613.

97. Just Kukurova I, Valkovič L, Bogner W, et al. Two-dimensional spectroscopic imaging with combined free induction decay and long-TE acquisition (FID echo spectroscopic imaging, FIDESI) for the detection of intramyocellular lipids in calf muscle at 7 T. *NMR Biomed*. 2014;27:980–987.

98. Phillips DI, Caddy S, Ilic V, et al. Intramuscular triglyceride and muscle insulin sensitivity: evidence for a relationship in nondiabetic subjects. *Metabolism*. 1996;45:947–950.

99. Pan DA, Lillioja S, Kriketos AD, et al. Skeletal muscle triglyceride levels are inversely related to insulin action. *Diabetes*. 1997;46:983–988.

100. Giraudo C, Motyka S, Weber M, et al. Diffusion tensor imaging of healthy skeletal muscles: a comparison between 7 T and 3 T. *Invest Radiol*. 2019;54:48–54.

101. Polders DL, Leemans A, Hendrikse J, et al. Signal to noise ratio and uncertainty in diffusion tensor imaging at 1.5, 3.0, and 7.0 Tesla. *J Magn Reson Imaging*. 2011;33:1456–1463.

102. Anderson JD, Epstein FH, Meyer CH, et al. Multifactorial determinants of functional capacity in peripheral arterial disease: uncoupling of calf muscle perfusion and metabolism. *J Am Coll Cardiol*. 2009;54:628–635.

103. Schewzow K, Fiedler GB, Meyerspeer M, et al. Dynamic ASL and T2-weighted MRI in exercising calf muscle at 7 T: a feasibility study. *Magn Reson Med*. 2015;73:1190–1195.